H1-08/88-90

Photon-Nucleon Interactions at H1

V.F.Andreev, A.I.Lebedev, I.P.Sheviakov and Yu.V.Soloviev
DESY/Lebedev Physical Institute, Moscow

1 Introduction

For the investigation of low Q^2-physics and for fast luminosity monitoring on the H1 detector at HERA, photon and electron calorimeters are under construction, consisting of Čherenkov counters [1].

It was necessary to test elements of these calorimeters, to develop a DAQ-system for them, to simulate hadron photoproduction events and to give a short outlook of recent motivations for the study of photon-nucleon interactions at high energies.

There was also need to suggest the method of checking the prototype of muon chamber pads, which will be used to detect decay muons from heavy flavour photoproduction and which will be placed in the iron yoke of the muon calorimeter.

The iron structure of the muon calorimeter is under assemmly in the HERA North Hall (fig.1). It is manufactured at Igora plant near Leningrad by contract with P.N.Lebedev Physical Institute. Two of three parts of this structure have been delivered already to DESY.

2 Topical problems of high energy photon-nucleon interactions

The increasing interest of studying the interaction of real or almost real photons with nucleon at high energies [2] is connected with the possibility to investigate in hard photon-hadron processes the QCD-dynamics and with the necessity of studying soft electromagnetic processes to develop realistic models of quark and gluon confinement. High energy photons can also be used as agent to produce both standard model particles (including t-quark) and new particles (SUSY, charged Higgs, etc.) [3].

First of all, it is necessary to measure the total photoabsorbtion cross section $\sigma_t(\gamma p)$ in the unexplored region of ultra high photon energies. The value $\sigma_t(\gamma p)$ is rather high ($\sim 100\mu b$). The tagged photon system of H1 [4] will give the possibility to measure $\sigma_t(\gamma p)$ at fixed proton target in $3 \div 34\ TeV$ energy interval. The $\sigma_t(\gamma p)$ measured at energies up to 200 GeV grows a little bit faster than VDM predicts [5]. The excess is probably due to jet production in photon-gluon fusion. There are also speculations on the considerable enhancement of $\sigma_t(\gamma p)$ at HERA energies because of the abundant gluon content of very high energy photons [6].

Data on $\sigma_t(\gamma p)$ will give possibility to obtain total hadron cross sections (for example πN) by use of VDM and additive quark model. It should be mentioned, that recent measurements of the real part of $\bar{p}p$-scattering amplitude create suggestions on unusual rise of hadronic cross sections at high energies [7,8] which also should manifested by VDM for $\sigma_t(\gamma p)$.

Conclusions about differential cross sections $d\sigma/dt$ for πN-scattering can be obtained from the ρ-photoproduction data. Unfortunately, the angle between pions from ρ-decay is very small at HERA energies, so it is difficult to detect light vector meson photoproduction, unless a large exitation is transfered to recoil nucleon. The conditions for investigation of heavy vector meson photoproduction is more suitable. The study of J/ψ-photoproduction will give possibility to measure gluon distribution function G(x) in nucleon at small x, where different parametrisations of G(x) lead to sizable derivations in the cross sections [2].

Heavy flavour production by photons is mainly due to photon-gluon fusion $\gamma g \to q\bar{q}$ which leads to the hadron jets production. It is necessary to study this process at HERA energies.

In the hadron fragmentation of produced partons in $\gamma g \to q\bar{q}$ subprocess there should be observed QCD interference effects. Coloured interference effects for a number of processes but not for ptotoproduction were predicted in the frame of string Lund model [9] and were explained in QCD terms in [10]. They were observed in the reactions $\epsilon^+\epsilon^- \to$hadrons [11]. It is very interesting to investigate the dynamics of QCD-coherence in hard processes of hadron photoproduction. Coherence effects lead to additional space asymmetry in hadron emission.

The search for new flavour will be one of the most exiting experiments at HERA. For the top masses up to $\sim$50 GeV photon-gluon fusion $\gamma g \to t\bar{t}$ gives the main contribution to the cross section of t-production by electrons [12,13]. To study the mechanisms of hadron photoproduction it is necessary to measure the energy dependence of corresponding cross section using tagged photon facility on H1. The detection in muon calorimeter of μ's from charm and beauty particles decay will be useful for picking out the heavy flavour photoproduction events.

The process of heavy flavour production in photon-gluon fusion can be also used to look for a charged Higgs bosons [14].

3 Monte Carlo simulation for hadron photoabsorbtion events

The expected number of hadron photoproduction events initiated by tagged photons in calorimeter is $3 \div 30\ s^{-1}$ [4]. Random coincidences between electrons in tagger and proton-gas interactions lead to a background of about 30 events/s. Thus, it is necessary to find such registration conditions which reduce the background in $10^2 \div 10^3$ times.

For this purpose MC simulation has been performed for the photoproduction and beam-gas interactions using LUCIFER 2.2 [15] and FRITIOF 1.7 [16] generators respectively. Two

kindes of residual gas were supposed: hydrogen and oxygen. Response of calorimeter was simulated by FLASH program [17] for H1.

The results on multiplicity triggers (at least one particle hits definite subdetector of the main H1 calorimeter) are presented in tab.1,2. It is seen that background in the backward part of the calorimeter is quite small. The following combinations of subdetectors were considered as possible triggers: TR1=BWE, TR2=$BWE + BBE$, TR3=$BWE + BBE + CB1$, TR4=$BWE+BBE+CB1+CB2$, TR5=$BWE+BBE+CB1+CB2+CB3$. It should be stressed that only above mentioned triggers are not enough to reduce the background to an acceptable level (tab.3).

According to MC simulation the deposited energy from background is considerably less than from photoproduction events in selected parts of the main calorimeter. As example energy distributions for TR5 are shown on fig.2. The different energy cuts give results enumerated in tab.4. One can conclude that when selecting low energy threshoulds it is possible to reduce background to an acceptable level without considerable decreasing of the registration efficiency for photoproduction events. In other cases a suitable trigger should be constructed according to specific physical prosess and to required rejection factor for background.

4 Detectors

It was proposed [4,18] to use two electromagnetic calorimeters for small angle electron tagging in $ep \to e'X$ events and for luminosity measurement by detecting of the QED process $ep \to e\gamma p$. Both calorimeters will have a cell structure. Each element of these detectors represents a Čerenkov shower counter with the $KRS-6$ crystal as radiator followed by a photomultiplier $PHEU-147$, having $\sim$ 15 mm diameter photocathode, as a readout. Main properties of $KRS-6$ as well as results of the MC simulation for the whole system are presented in [1,4].

In order to check our expectations concerning the main features of the detectors two small calorimeter prototypes were built and tested. The main tasks were to study an energy and space resolutions of prototype and to examine detector response as a function of electron (or photon) impact point.

First prototype consisting of 2×2 elements was tested at DESY in the electron beam at energies up to 4.5 GeV. The size of the beam spot at the entrance window of the detector had been determined by crossing of two scintillation counters both of 2 mm width. The calorimeter was placed on the movable table that allowed electron beam to scan a front surface of the prototype.

To determine an energy deposition in calorimeter it is necessary to know calibration coefficients C_i for all calorimeter channels:

$$E_0 = \sum_i C_i A_i,$$

where E_0 is deposited energy and A_i - amplitude in the i-th channel.

During the data processing the calibration coefficients were being determined by minimization of a value

$$\sum_j (P_0 - \sum_i C_i A_{ij})^2,$$

where P_0 is a mean value of electron beam momentum, and j is event number.

An electron impact coordinates (X, Y) were being calculated using relation

$$(X,Y) = \sum_i (XC_i, YC_i) F(f_i),$$

where (XC_i, YC_i) - coordinates of the centers of calorimeter elements, $f_i = E_i/E_0$, E_i - deposited energy in the i-th element, E_0 - total energy deposited: $E_0 = \sum E_i$, $F(f_i)$ - function reflecting a lateral shower development.

The main results of the test measurements are illustrated by fig.3-6. Fig.3 shows that the dependence of energy resolution on E_e in the $1 \div 4.5$ GeV range differs from the expected one for the $5 \div 30$ GeV range, for which our detectors had been optimized [1].

For correct electron (photon) energy reconstruction it is necessary to know a detector response as a function of impact point coordinate. This dependence is shown on fig.4. As it is seen, the calorimeter response falls down by a value of 8% at a distance $\sim$ 10 mm from detector boundaries. Moreover, near the split between adjacent elements (x=0) the detector response also decreases on the same value.

The function of a lateral development of electromagnetic shower in $KRS-6$ is presented on fig.5. This function was determined in the first test run, and afterwards it was used for calculation of the electron impact point coordinates.

The accuracy of an impact point coordinates reconstruction can be extracted from the Δx-distribution, shown on fig.6. Here $\Delta x = x_t - x_c$; x_t is a coordinate of the electron beam center on the front surface of prototype, measured by remote control indicator of a movable table, and x_c is the same coordinate, but measured by the calorimeter prototype according to the algorithm, described above. Both x_t and x_c had been measured relatively the same initial point. The obtained value of coordinate reconstruction accuracy $\sigma_{x,y}$ is about 0.6 mm, which is close to expected space resolution [4].

5 Triggers and DAQ for luminosity monitoring and electron tagging

Small angle e^-- and γ-detectors have two separate functions: luminosity monitoring and tagging of the low Q^2 events. These tasks require two triggering and DAQ systems.

For building low Q^2 trigger it is foreseen to send the electron trigger to the central one for combining with other H1 triggers. The trigger from the tagger logic must reach the central trigger unit at a fixed time relative to the beam crossing moment. The readout will then occur in the same way as for the tracking data.

To form the bremsstrahlung trigger for the luminosity measurement it is foreseen to create special system which will count events satisfying an appropriate coinsidence between the electron tagger and the forward γ-detector. This function needs no connection with the central trigger and DAQ at the single event level. It is anticipated that the trigger will be initially hardware based on discriminator outputs and relevant clusters finding in two detectors. The luminosity data must be read both more frequently and completely out of synchronism with the main H1 data. Hence, a quite separate readout channels would be needed for the detecting photoproduction and for luminosity monitoring. For this reason the

[1] The second 3×3 calorimeter prototype was tested on the e^--beam of the Serpukhov accelerator up to $E_e = 28 GeV$. The data are under processing.

corresponding data will be put into two separate FADC crates which have be controlled by different processors in order to extract only the relevant data.

The block diagram of the first level luminosity monitoring and electron tagger triggers is shown on fig.7. Details on the method of triggering and data aquisition can be found in [19].

6 Method for checking muon chamber pads

It was proposed and experimentally investigated one of the methods for serial checking of various electrical characteristics of the muon chamber pads. The method is based on the determination of discrepancy between the reference pad and the pad to be chacked. The value of difference is determined by comparing of high frequency and low frequency responses of both pads. The using of two frequencies allows to compare capacitance and resistance characteristics simultaneously. It was found that all distinctions can be measured within $\sim 2\%$ accuracy. To check whole pad structure it is sufficient to have only one reference pad per family. The scanning and measuring procedures have of course operate under computer control.

7 Conclusion

It should be mentioned that radiative corrections to deep inelastic scattering at HERA will play an essential role [20,21]. Electron and photon detectors developed for luminosity monitor can be used to measure these corrections and considerably reduce the uncertainty of QCD check at high Q^2.

References

[1] Technical Progress Report. *H1 Collaboration, Oct.4, 1987.*

[2] Diekmann B. et al. Workshop Physics at HERA, *1987.*

[3] Wolf G. DESY 86-089, *1986.*

[4] Levonian S.V. et al. H1-TR 113, Oct.13, *1987.*

[5] Caldwell D. et al. Phys.Lett. B **40**. p.1222, *1978.*

[6] Drees M., Halzen F. MAD/PH/408. *1988.*

[7] Kluit P.M., Timmermans J. NIKHEFF-H-187-22, *Dec., 1987.*

[8] Hadjitheodoridis S., Kang K. CERN-TH-5000/88, *1988.*

[9] Anderson B., Gustafson G. Phys.Rep.,**97**, p.33, *1983.*

[10] Dokshitzer Yu.L. et al. Rev.Mod.Phys., **60**, p.373, *1988.*

[11] Bartel W. et al. Phys.Lett. B **101**, p.129, *1981.*

[12] Ingelman G., Schuler G.A. DESY 88-020, *1988.*

[13] Eichler R.A., Kunszt Z. ETHZ-IMP P/88-1, *1988.*

[14] Grzadkowski B., Hov Wei-Shu MPI-PAE/PTh 14/88, *1988.*

[15] Ingelman G., Weigend A. CPC, **46** p.241,*1987.*

[16] Nilsson-Almquist B., Stenlund E. CPC, **43**, p.387, *1987.*

[17] Grindhammer G., Mundt R., Rudowicz M., H1-09/87-71, *1987.*

[18] Belousov A.S. H1-10/86-54, *1986.*

[19] Andreev V.F. et al. H1-05/88-86, *1988.*

[20] Bardin D.Yu. et al. JINR, E2-87-595, Dubna, *1985.*

[21] Kripfganz J., Möhring H.J. Z.Phys. C **38**, p.653, *1988.*

Figure Captions

Fig. 1 Assemling of the H1 iron structure in HERA North Hall (Aug. 1988).

Fig. 2 Deposited energy distributions in TR5 for the photoproduction events (full histogram) and background (dotted one).

Fig. 3 Dependence of energy resolution HWHM on mean value of electron beam energy.
● - test measurements in Moscow at energies 0.5 and 0.6 GeV,
○ - without substraction of the beam energy spread,
■ - with substraction of beam energy spread.
The curve represents an expected behavior of energy resolution [4].

Fig. 4 Detector response as a function of impact point of electron.
X=0 corresponds to the boundary between two adjacent elements.

Fig. 5 Function of the lateral shower development.
X=0 corresponds to the center of prototype,
E_0 - total energy deposited,
E_1 - energy deposited in two elements in vertical row.

Fig. 6 Coordinate reconstruction accuracy for the prototype (see text).

Fig. 7 Block diagram for the first level triggers.

Multiplicity ≥ 1			
Reaction	g-P	p-O	p-P
ALL.	1.000	1.000	1.000
PLU.	0.954	0.936	0.880
FOR.	0.979	0.969	0.946
BAR.	0.991	0.979	0.966
FBC.	0.838	0.867	0.761
CBC.	0.965	0.831	0.725
CB3.	0.517	0.505	0.361
CB2.	0.706	0.356	0.214
CB1.	0.777	0.160	0.089
BBE.	0.461	0.023	0.012
BWE.	0.950	0.024	0.013

Table 1. Geometrical acceptence for the different parts of calorimeter.

Multiplicity ≥ 2			
Reaction	g-P	p-O	p-P
ALL.	1.000	0.993	0.985
PLU.	0.848	0.881	0.780
FOR.	0.919	0.922	0.858
BAR.	0.966	0.850	0.697
FBC.	0.621	0.685	0.478
CBC.	0.889	0.523	0.270
CB3.	0.173	0.145	0.026
CB2.	0.395	0.090	0.022
CB1.	0.497	0.019	0.004
BBE.	0.151	0.0003	0.000
BWE.	0.838	0.0002	0.000

Table 2. Gegometrical acceptence for the different parts of calorimeter.

$N \geq 1$	TR1	TR2	TR3	TR4	TR5
(g-P)	0.950	0.967	0.988	0.995	0.997
(p-O)	0.024	0.047	0.195	0.463	0.748
(p-P)	0.013	0.025	0.110	0.300	0.608
$N \geq 2$	TR1	TR2	TR3	TR4	TR5
(g-P)	0.716	0.742	0.806	0.844	0.884
(p-O)	0.0002	0.001	0.030	0.165	0.367
(p-P)	0.000	0.0002	0.007	0.054	0.121

Table 3. Efficiencies of the different triggers

$E \geq 0.$	TR1	TR2	TR3	TR4	TR5
(g-P)	0.975	0.982	0.991	0.996	0.997
(p-O)	0.005	0.009	0.027	0.158	0.574
(p-P)	0.003	0.004	0.017	0.092	0.394
$E \geq 1.$	TR1	TR2	TR3	TR4	TR5
(g-P)	0.883	0.890	0.915	0.946	0.962
(p-O)	0.000	0.000	0.000	0.000	0.012
(p-P)	0.000	0.000	0.000	0.000	0.0005
$E \geq 2.$	TR1	TR2	TR3	TR4	TR5
(g-P)	0.752	0.774	0.798	0.847	0.869
(p-O)	0.000	0.000	0.000	0.000	0.000
(p-P)	0.000	0.000	0.000	0.000	0.000

Table 4. Efficiencies of the different triggers

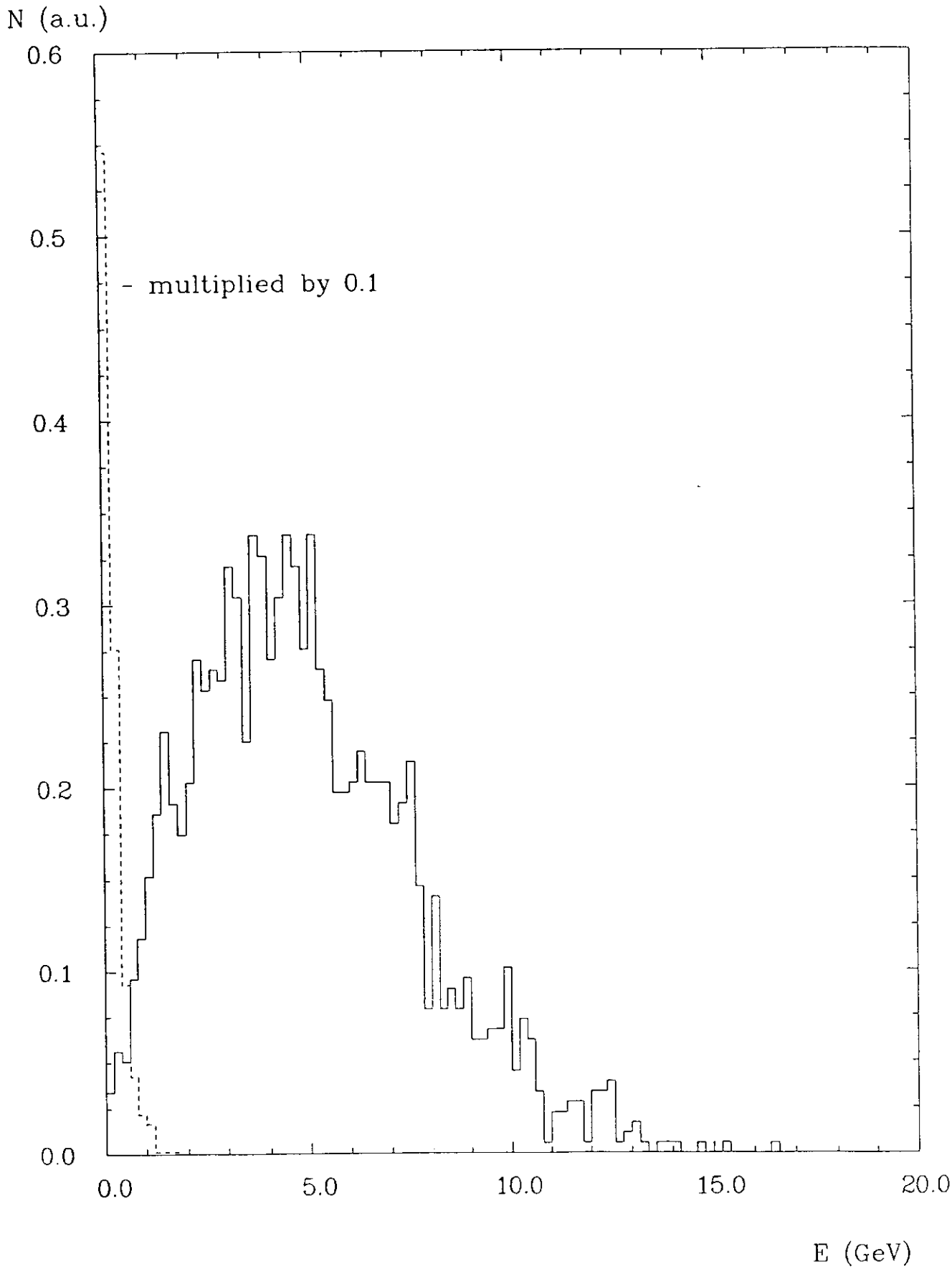

Fig.2

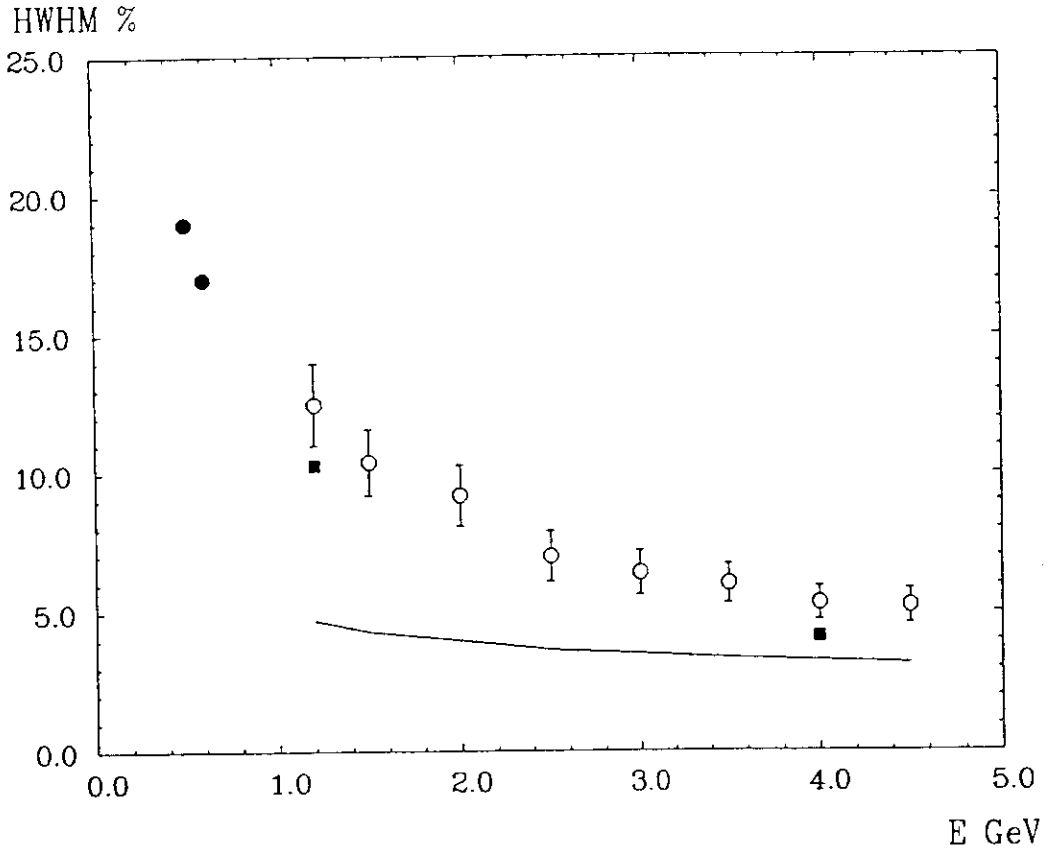
HWHM %
25.0
20.0
15.0
10.0
5.0
0.0
0.0
1.0
2.0
3.0
4.0
5.0
E GeV

Fig.3

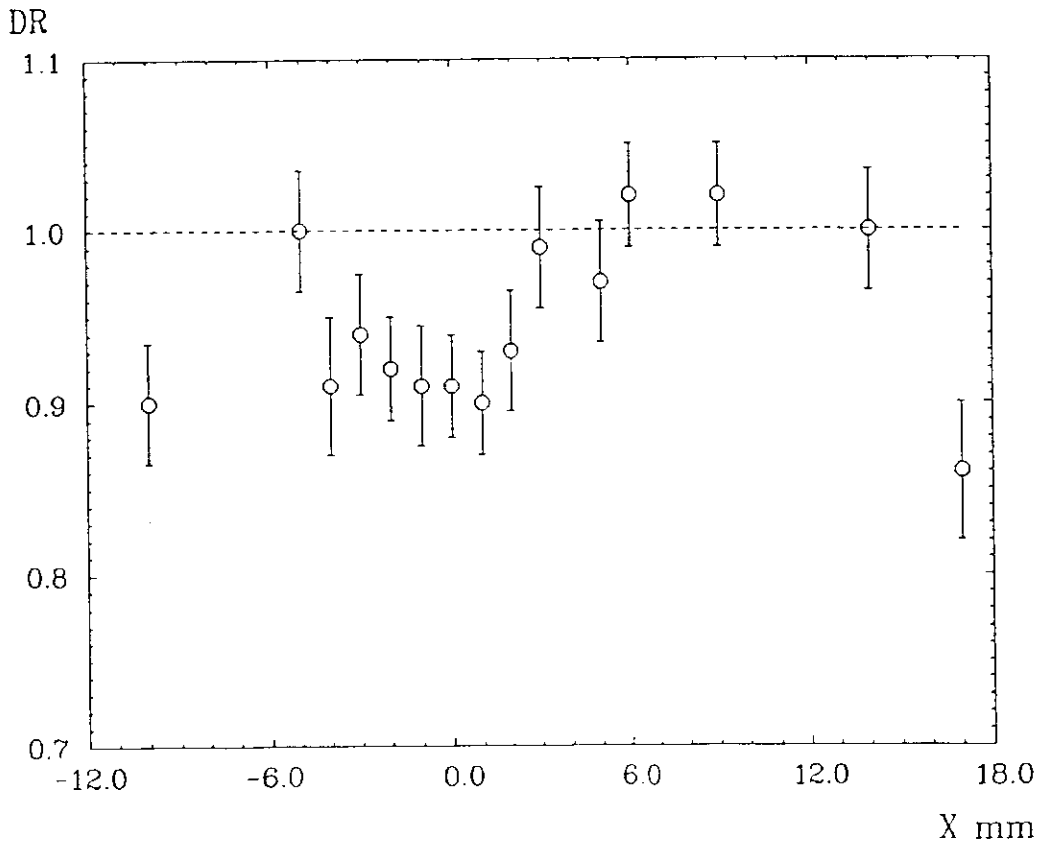
DR
1.1
1.0
0.9
0.8
0.7
-12.0
-6.0
0.0
6.0
12.0
18.0
X mm

Fig.4

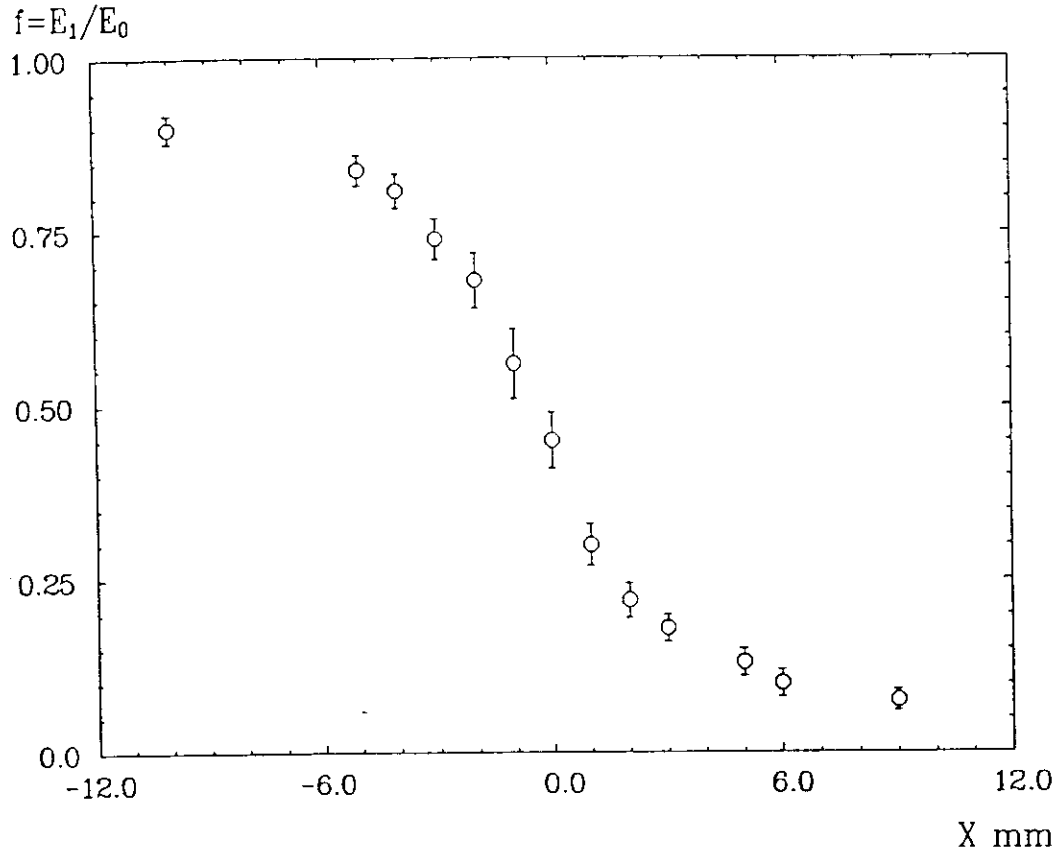
f=E1/E0
1.00
0.75
0.50
0.25
0.0
-12.0
-6.0
0.0
6.0
12.0
X mm

Fig.5

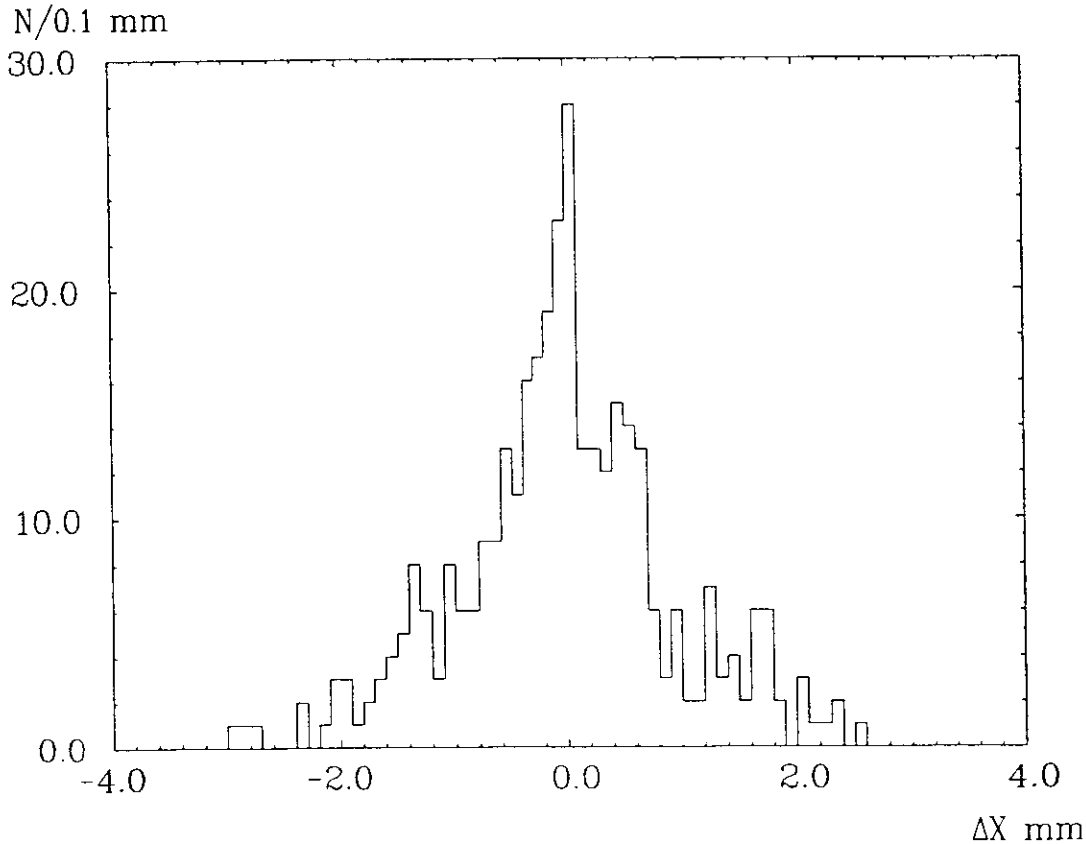
N/0.1 mm
30.0
20.0
10.0
0.0
-4.0
-2.0
0.0
2.0
4.0
ΔX mm

Fig.6

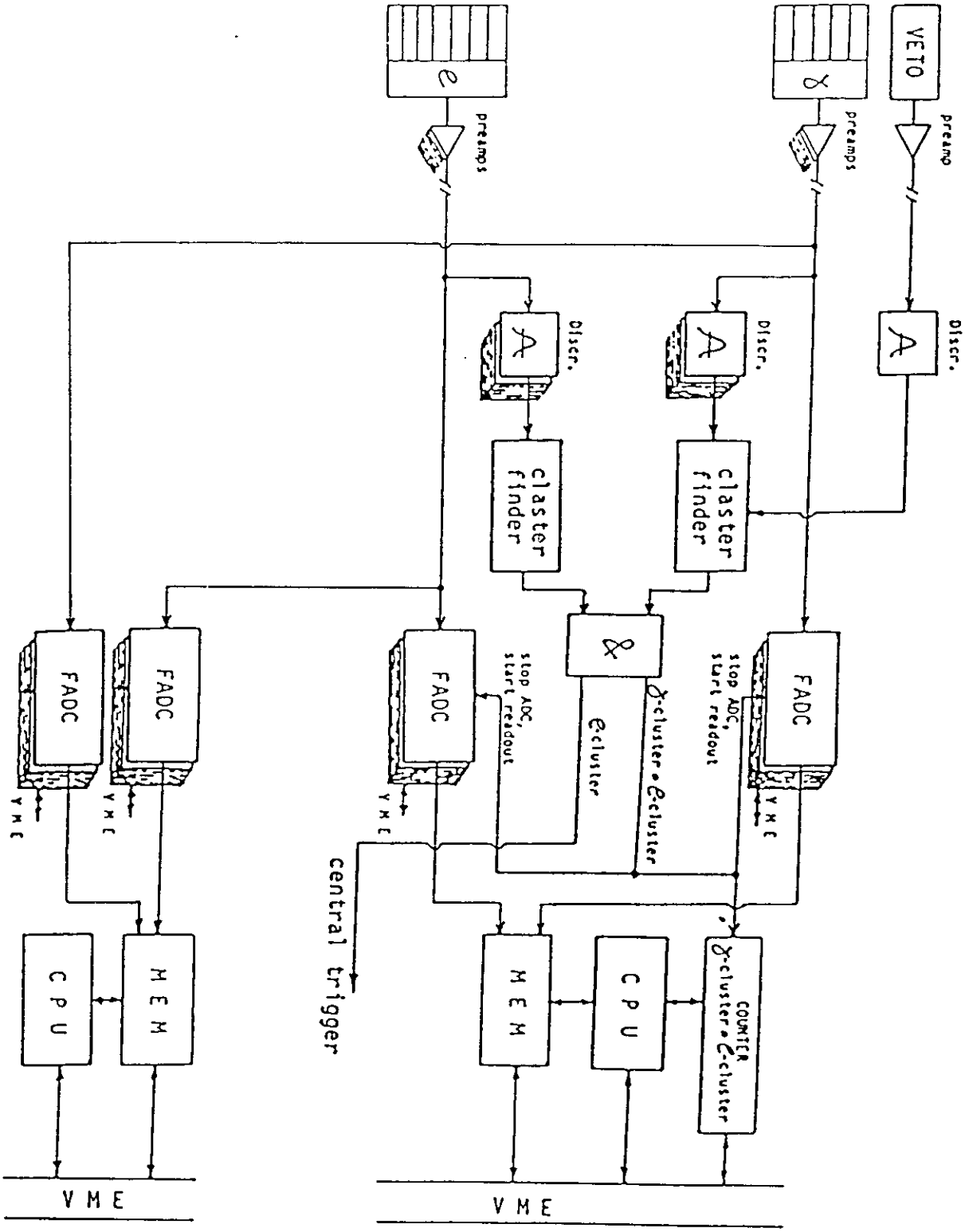
VETO
preamp
Discr.
preamps
Discr.
preamps
Discr.
claster finder
claster finder
&
stop ADC, start readout
stop ADC, start readout
e-cluster
γ-cluster • e-cluster
FADC
FADC
FADC
FADC
VME
VME
VME
VME
central trigger
CPU
MEM
CPU
MEM
COUNTER γ-cluster • e-cluster
VME
VME

Figure 7.

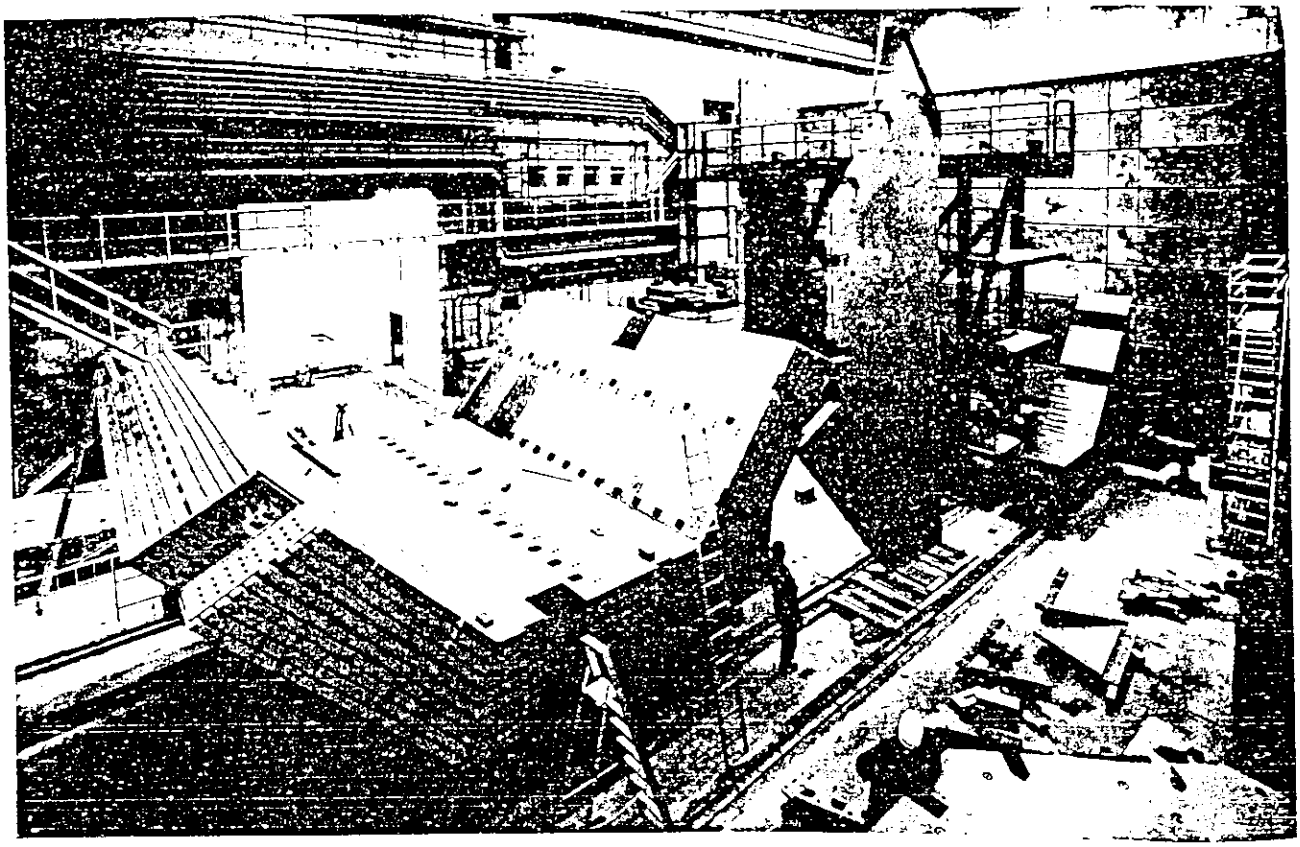

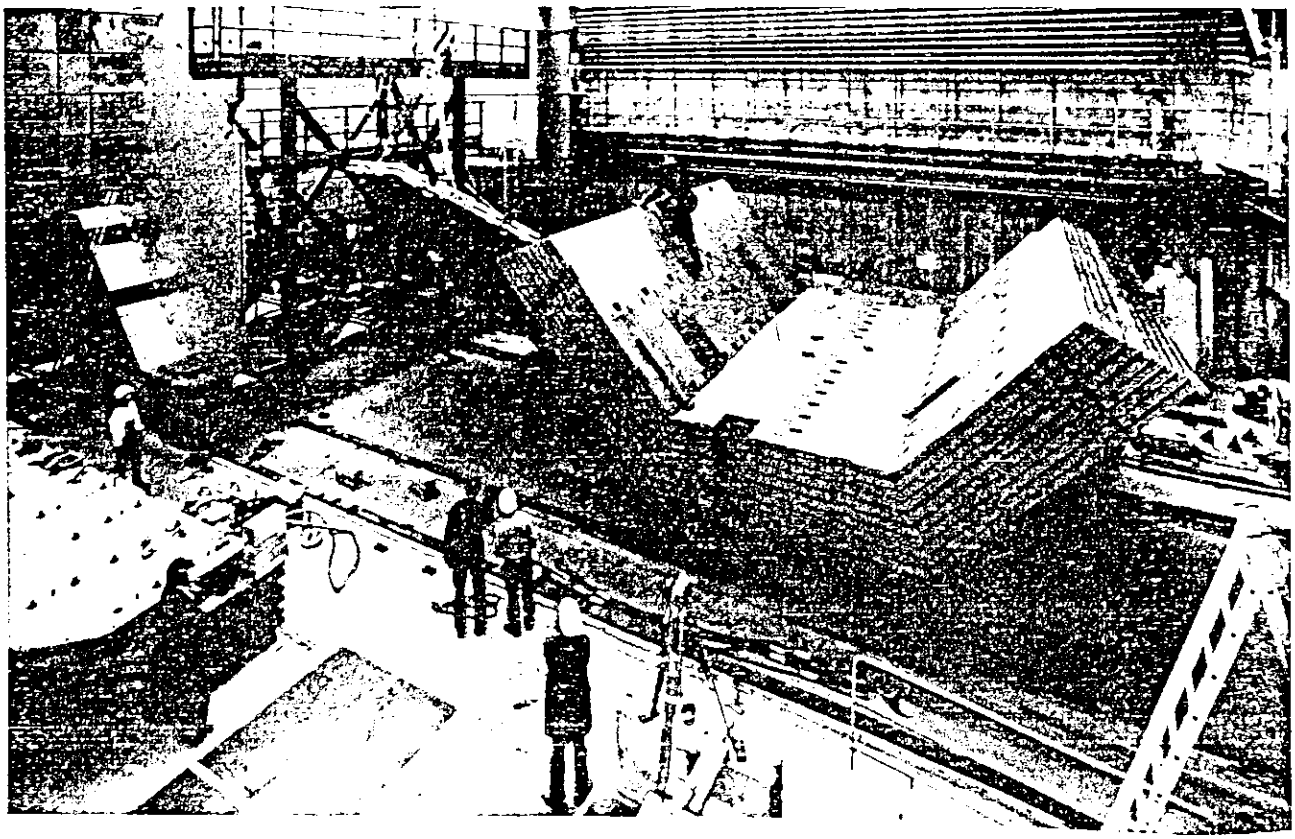

Fig. 1